AIP | The Journal of Chemical Physics

A comprehensive and comparative study of elastic electron scattering from OCS and CS2 in the energy region from 1.2 to 200 eV

H. Murai, Y. Ishijima, T. Mitsumura, Y. Sakamoto, H. Kato et al.

Citation: J. Chem. Phys. **138**, 054302 (2013); doi: 10.1063/1.4788666
View online: http://dx.doi.org/10.1063/1.4788666
View Table of Contents: http://jcp.aip.org/resource/1/JCPSA6/v138/i5
Published by the American Institute of Physics.

A comprehensive and comparative study of elastic electron scattering from OCS and CS_2 in the energy region from 1.2 to 200 eV

H. Murai,[1] Y. Ishijima,[1] T. Mitsumura,[1] Y. Sakamoto,[1] H. Kato,[1] M. Hoshino,[1,a)] F. Blanco,[2] G. García,[3] P. Limão-Vieira,[1,4] M. J. Brunger,[5,6] S. J. Buckman,[6,7] and H. Tanaka[1]
[1]*Department of Physics, Sophia University, Tokyo 102-8554, Japan*
[2]*Departamento de Fisica Atomica, Molecular y Nuclear, Facultad de Ciencias Fisicas, Universidad Complutense de Madrid, E-28040 Madrid, Spain*
[3]*Instituto de Matemáticas y Física Fundamental, Consejo Superior de Investigaciones Científicas, 28006 Madrid, Spain*
[4]*Laboratório de Colisões Atómicas e Moleculares, CEFITEC, Departamento de Física, Faculdade de Ciências e Tecnologia, Universidade Nova de Lisboa, 2829-516 Caparica, Portugal*
[5]*ARC Centre for Antimatter-Matter Studies, Flinders University, G.P.O. Box 2100, Adelaide, South Australia 5001, Australia*
[6]*Institute of Mathematical Sciences, University of Malaya, 50603 Kuala Lumpur, Malaysia*
[7]*ARC Centre for Antimatter-Matter Studies, Australia National University, Canberra, ACT 0200, Australia*

(Received 20 December 2012; accepted 7 January 2013; published online 1 February 2013)

We report absolute differential cross sections (DCSs) for elastic electron scattering from OCS (carbonyl sulphide) and CS_2 (carbon disulphide) in the impact energy range of 1.2–200 eV and for scattering angles from 10° to 150°. Above 10 eV, the angular distributions are found to agree quite well with our present calculations using two semi-phenomenological theoretical approaches. One employs the independent-atom model with the screening-corrected additivity rule (IAM-SCAR), while the other uses the continuum-multiple-scattering method in conjunction with a parameter-free exchange-polarization approximation. Since OCS is a polar molecule, further dipole-induced rotational excitation cross sections have been calculated in the framework of the first Born approximation and incoherently added to the IAM-SCAR results. In comparison with the calculated DCS for the S atom, atomic-like behavior for the angular distributions in both the OCS and CS_2 scattering systems is observed. Integrated elastic cross sections are obtained by extrapolating the experimental measurements, with the aid of the theoretical calculations, for those scattering angles below 10° and above 150°. These values are then compared with the available total cross sections. © *2013 American Institute of Physics*. [http://dx.doi.org/10.1063/1.4788666]

I. INTRODUCTION

The present experimental results for OCS (carbonyl sulphide) and CS_2 (carbon disulphide) complete our objective in providing differential cross section (DCS) measurements for elastic electron scattering from linear tri-atomic molecules, such as HCN,[1] CO_2,[2] and N_2O.[3] Studies on OCS have attracted considerable attention from the scientific community because it plays an important role in the global sulphur cycle, along with other sulphur containing molecules found in seawater namely, $(CH_3)_2S$ and $(CH_3)_2SO$.[4,5] These molecules, while being precursors of sulphate aerosol particles and cloud condensation nuclei, can act as a feedback mechanism in climate regulation, affecting the Earth's radiative balance by direct scattering of solar radiation. OCS is also a source of biogenic sulphur,[6–10] and has been detected in the interstellar medium and in the upper atmospheres of Venus and Jupiter.[11–14] Recently, the quantitative assessment of sulphur isotope distributions in geological samples through UV absorption has provided a record of atmospheric composition, indicating the role of OCS in the radiative forcing of the former Archaen atmosphere.[15] OCS is also used technologically as a new additive gas for fine etching of semiconductors in low-temperature plasmas.[16] From an astronomical point of view, the identification of the UV-visible spectra from CS, C and S emissions from comets has attracted the study of the stable parent molecule, CS_2, of those atomic and radical species.[17] From the quantum chemical point of view, CO_2, OCS, and CS_2 have been investigated extensively as they form a series of closely related triatomic linear molecules. Their electronic ground-state configurations are similar, but their dipole polarizabilities vary significantly, being 19.6 a.u. for CO_2, 38.5 a.u. for OCS, and 59.8 a.u. for CS_2.[18] In addition, only OCS has a permanent dipole moment of 0.715 D.[19] The sulphur atoms in CS_2, with low-lying *d* orbitals, have a significant influence on the chemical bonding as well as a prominent role in the ionization dynamics of the molecule.[20]

As far as electron collisions with OCS and CS_2 are concerned, a literature survey allows us to briefly summarize the elastic differential and integral cross sections, as well as the grand total (elastic + inelastic) cross sections as follows.

For OCS: Total cross sections have been measured by Szmytkowski *et al.* (impact energy E_0 = 0.2–100 eV),[21,22] Dababneh *et al.* (E_0 = 0.8–40 eV),[23] Zecca *et al.*

a)Author to whom correspondence should be addressed. Electronic mail: masami-h@sophia.ac.jp. Tel: (+81) 3 3238 4227. Fax: (+81) 3 3238 3341.

(E_0 = 90–4000 eV),[24] Sueoka *et al.* (E_0 = 0.8–600 eV),[25] and Jones *et al.* (E_0 = 0.015–2.5 eV).[26] The elastic differential cross sections were measured by Sohn *et al.* (E_0 = 0.3–5 eV, for scattering angles θ = 12.5°–138°),[27] Sakamoto *et al.* (E_0 = 1.5–100 eV, θ = 20°–130°),[28] and Hoffmann *et al.* (E_0 = 0.06–20 eV, θ = 135°).[29] Integral elastic cross sections have been obtained by Sohn *et al.* (E_0 = 0.4–5 eV),[27] and Sakamoto *et al.* (E_0 = 1.5–100 eV).[28] Differential, integral elastic, and momentum transfer cross sections have been calculated by using the independent atom model (IAM) at intermediate energies of 100–1000 eV[30] whereas the integral elastic cross section, calculated using the continuum multiple-scattering model from 0 to 100 eV, has been reported by Lynch *et al.*[31] The elastic DCS and ICS were also calculated by Bettega *et al.*[32,33] Gianturco and Stoecklin,[34] Michelin *et al.*,[35] and Heng *et al.* (E_0 = 200–1000 eV, θ = 20°–130°).[36] Finally, the total cross section was calculated above 200 eV by Raj and Tomar,[30] who have employed an optical model approach.

For CS_2 the total cross section has been measured by Szmytkowski, at impact energies from 0.2 to 80 eV,[37] and by Jones *et al.* from a few meV to a few hundred meV impact energy.[38] Elastic differential cross sections were measured by Sohn *et al.* (0.3–5 eV, and for scattering angles θ = 12.5°–138°),[27] Sakamoto *et al.* (E_0 = 1.5–100 eV, θ = 20°–130°),[28] and Allan (E_0 = 1–12 eV, θ = 135°).[39] Integral elastic cross sections were obtained by Sohn *et al.* (E_0 = 0.3–5 eV)[27] and Sakamoto *et al.* (E_0 = 1.5–100eV).[28] Theoretical studies of the integral elastic cross section have been performed by Lynch *et al.* (E_0 = 0.4–1000 eV),[31] using the continuum multiple-scattering model. Szmytkowski (E_0 = 1–100 eV)[40] performed a two-centre, parametric optical potential calculation for differential, integral elastic, and momentum transfer cross sections. Raj and Tomar (E_0 = 100–1000 eV)[30] have employed the IAM, while Lee *et al.* (E_0 = 0.04–100 eV)[41] have made use of the Schwinger variational iterative (SVIM) method using the distorted-wave approximation. Schwinger multichannel (SMC) calculation results at both the static exchange (SE) and static exchange plus polarization (SEP) levels have also been reported by Bettega *et al.*,[42,43] with a further computation from Gianturco and Stoecklin[44] also being noted.

In the present work we have conducted a comprehensive, combined experimental-theoretical study on OCS and CS_2. It is worth noting that although our present data on OCS has been cited partially in comparison with the computational methods available,[32–35] the complete set of cross sections in this report have not been presented in detail from an experimental point of view. As such, new measurements are compared with the existing experimental and theoretical data below 3 eV and above 100 eV. Also, following on from our series of studies on "atomic-like" effects which appear to prevail in high-energy electron scattering from molecules,[45–48] we further extend this study by comparing the elastic DCSs for OCS and CS_2, where collisions with atomic sulphur appear to dominate the scattering dynamics. Further evidence lending support to this behavior is demonstrated by our IAM-SCAR results. This paper is organized as follows. In Sec. II, we describe briefly the experimental setup and procedure. In Sec. III, a brief description of the present IAM-SCAR computations is provided. Section IV is devoted to the results and discussion and we conclude with a short summary.

II. EXPERIMENT

The present experiments were performed with two electron spectrometers that have been described in detail in previous papers (e.g., Tanaka *et al.*[49] and Kato *et al.*[46]). Briefly, in both systems, the main features are a crossed electron-molecular beam arrangement, incorporating hemispherical monochromators and analyzers, electron lens systems with computer-driven voltages, and differential pumping for the electron optics. One of these experiments has been designed to be used at higher impact energies (>50 eV), with access to the larger scattering angles up to 150° which is gained by operating it at a somewhat lower energy resolution. As far as the impact energy range is concerned, the first (high resolution) apparatus covers the range from 1.2 to 60 eV and an angular range from −20° to +130°, whereas the second (lower resolution) apparatus allows an energy range from 100 to 200 eV and an angular range from −20° to 150°. The overall energy resolution was 35 meV (FWHM - high resolution) or 90 meV (FWHM - low resolution).

The vibrational fundamental modes, whose energy spacing in both OCS (ν_1: 107 meV, ν_2: 64.5 meV, ν_3: 256 meV) and CS_2 (ν_1: 81 meV, ν_2: 49 meV, ν_3: 190 meV)[50] means they can of course be excited in both apparatus, might also make some contribution (together with rotational excitation) to the elastic scattering intensity. With the present energy resolution these modes can only be partially resolved in the low energy (high resolution) apparatus, and rotational effects cannot be resolved at all. In the low energy (high resolution) measurements we thus measure a rotationally summed elastic DCS, while in the high energy (low resolution) measurements; we expect the contributions from both vibrational and rotational excitation to be negligible. In each case such small contributions are expected to exert very little influence on the shape or magnitude of the elastic DCS.

The energy scale was calibrated by reference to the 19.365 eV resonance in He,[51] and the quasi-vibrational $\nu = 0 \rightarrow 1$ peak of N_2^-, which occurs in elastic scattering at an incident energy of 1.97 eV.[52] In both spectrometers the angular scale zero was determined from the symmetry of the angular distribution for excitation of He 2^1P about the nominal 0° scattering angle, with an angular resolution estimated to be ±1.5°. The molecular beam was produced effusively from a simple tube nozzle (L = 5 mm, D = 0.3 mm), kept at slightly elevated temperatures (50–70 °C) throughout the measurements in order to avoid the contamination of OCS and CS_2 on the nozzle surface.

The measured intensities of elastically scattered electrons were converted into absolute cross sections by use of the relative flow technique,[53,54] combined with the known DCSs of He.[55] It requires adjustment of the gas driving pressures to obtain equal Knudsen numbers in the beam-forming tube, so that the gas beam profiles remain similar. The actual head pressures behind the nozzle were about 3 Torr for He, 0.5 Torr

for OCS, and 0.3 Torr for CS_2, respectively. There have been persistent reports in the literature of nonlinearity in plots of the gas flow-rate versus head pressure,[56,57] even for simple gases like N_2. However, all these reports refer to capillary nozzles. We were not able to reproduce such nonlinearities with the present equipment.

Finally, we note that the overall uncertainties on the measured elastic DCS lie in the range 15%–20% with the largest component of the error being due to the uncertainty in the cross sections of the helium reference gas (∼20%).

III. THEORETICAL OUTLINE AND NUMERICAL ANALYSIS

In order to obtain a better understanding of our experimental results, we have calculated the e-OCS and –CS_2 elastic cross sections by using the screening corrected independent atom scattering method (IAM-SCAR) as well as the continuum multiple-scattering (CMS) method as a supplemental tool for carrying out the analysis. Both methods have been proven to be a reasonably successful tool for reproducing experimental observations at higher energies, not only for electron-polyatomic molecule collisions, but also in electron-diatomic molecules. In particular, the methods are useful for studying larger molecules where *ab initio* theoretical approaches are not readily applicable due to the required extensive computer time. Given the previous discussion of these techniques in the literature, a brief description will suffice for the present purposes.

In the IAM-SCAR approach,[58–62] the first subjects of the present calculations are the atoms constituting the molecules in question, namely C, O, and S. We represent each atomic target by an interacting complex potential (the so-called optical potential), whose real part accounts for the elastic scattering of the incident electrons, while the imaginary part represents the inelastic processes which are considered as "absorption" from the incident beam. To construct this complex potential for each atom, we followed the procedure proposed by Staszewska *et al.*,[63] where the real part of the potential is represented by the sum of three terms: (i) a static term derived from a Hartree–Fock calculation of the atomic charge density distribution,[64] (ii) an exchange term to account for the indistinguishability of the incident and target electrons,[65] and (iii) a polarization term[66] for the long-range interactions which depends on the target polarizability α.[18] The imaginary part then treats inelastic scattering as electron-electron collisions. However, we initially found some important discrepancies with the available experimental atomic scattering data, which were subsequently corrected when a correct formulation of the absorption potential[58] was introduced. Further improvements to the original formulation,[63] such as the inclusion of screening effects and in the description of the electron's indistinguishability,[59] finally led to a model which provides a good approximation for electron-molecule scattering over a very broad energy range.[46–48]

To calculate the cross sections for electron scattering from molecules, we follow the IAM by applying a coherent addition procedure, commonly known as the additivity rule (AR). In this approach, the molecular scattering amplitude is derived from the sum of all the relevant atomic amplitudes, including the phase coefficients, therefore leading to the molecular DCSs for the molecule in question. ICSs can then be determined by integrating those DCSs. Alternatively, ICSs can also be derived from the relevant atomic ICSs in conjunction with the optical theorem.[59] Unfortunately, in its original form, we found an inherent contradiction between the ICSs derived from these two approaches, which suggested the optical theorem was being violated.[67] We, however, solved this problem by employing a normalization procedure during the computation of the DCSs, so that ICSs derived from the two approaches are now entirely consistent.[67] A limitation with the AR is that no molecular structure is considered, so that it is really only applicable when the incident electrons are so fast that they effectively only see the target molecule as a sum of the individual atoms (typically when above about 100 eV). To reduce the effect of that limitation, we introduced the SCAR method,[60,61] which considers the geometry of the relevant molecule (atomic positions and bond lengths) by employing some screening coefficients. With this correction the range of validity can be extended to incident electron energies as low as about 30 eV. For intermediate and high energies, this method has proven to be a powerful tool to calculate electron scattering cross sections from a high variety of molecules of very different sizes, from diatomic to complex biomolecules.[68] Moreover, this approach seems to be inherently suitable for electron scattering from a heavy atom-rich molecule, such as GeF_4, in which its application ranges down to 7 eV.[48]

Furthermore, for the polar molecule OCS, additional dipole-excitation cross sections can be calculated through the IAM-SCAR and rotational contribution method[62,69] which has been successfully used for other polar molecules such as H_2O.[70] Thus, the range of validity of our approach may be extended to energies possibly below 10 eV.

In the present application all model improvements described above have been implemented in our DCS and ICS computations, for all species, at each energy considered. We note, however, that the present calculations revealed that contributions from the dipole moment, for OCS, are only significant for scattered electron angles below 10°, which were not experimentally accessed in the present measurements. Importantly, those calculations were nonetheless used to obtain ICS in our extrapolation procedure.

In the CMS calculation,[71,72] to overcome difficulties arising from (i) the many degrees of freedom of electronic and nuclear motions and (ii) the nonspherical molecular field in the polyatomic molecule, the molecular configuration space is partitioned into three regions, each with a corresponding potential. Those regions are the atomic spheres (region I), the interstitial region (region II), and the spherical region surrounding the whole molecule (region III). The scattering part of the method is based on the static-exchange-polarization potential model within the fixed-nuclei approximation. The static interaction is constructed from the electron density obtained from the discrete variational Xα method of Averill and Ellis.[73] The Hara-type free-electron gas model[74] is employed for the local-exchange interaction, while the dipole and polarization interactions are treated via terms proportional to r^{-2} and r^{-4},

respectively. A simple local-exchange potential replaces the more cumbersome nonlocal exchange potential, making the calculation tractable. After solution of the Schrödinger equation in each region, the scattering S-matrix is determined by continuity conditions at the bounding surfaces. Once the S-matrix is known, then the scattering cross-section can be easily calculated. This approach has been tested extensively and is known to provide useful information on the underlying scattering physics. Furthermore, the CMS method is also useful for interpolation and extrapolation of the experimental data, as is discussed below.

The present measurements were limited to the angular range of 15°–130° for energies below 60 eV, and between 15° and 150 ° for energies above 100 eV. The measured DCSs were thus extrapolated to 0° and to 180° with the help of the present CMS and IAM-SCAR calculations. This approach was also confirmed by applying the Schwinger variational iterative method to crosscheck those extrapolated values, especially, at the lower impact energies. We note that the sole purpose of these extrapolations is to obtain the integral elastic cross sections from the DCS data, with a reasonable estimate for that part of the DCS that cannot be measured below 10° and above 130° or 150° in the present work. Please further note that the percentage contributions to our derived ICS, from the angular DCS regions we could not experimentally access, varied from ∼30% at 4 eV to ∼61% at 200 eV, for OCS, and varied from ∼17% at 3 eV to ∼66% at 150 eV in CS_2. As far as the ICS is concerned, this has been estimated as follows;

$$Q_e(E) = 2\pi \int DCS(\theta) \sin\theta d\theta. \quad (1)$$

The uncertainties on the derived values for Q_e are estimated to be about 25%–30%.

IV. RESULTS AND DISCUSSION

The experimental and theoretical results regarding the elastic DCS, elastic ICS, and TCS, for both OCS and CS_2, are shown in Figures 1–6 and are presented in Tables I and II.

A. OCS

Figure 1 is intended to give an overall view of the evolution of the angular behavior and magnitude of the elastic DCS across the energy range. It shows the measured absolute elastic cross sections at electron impact energies from 1.2 to 60 eV for scattering angles of 15° to 130°, and from 100 eV to 200 eV for scattering angles between 15° and 150°. The present calculated results (IAM-SCAR and CMS) are also plotted (the full blue and red dotted curves, respectively) from 1.5 eV to 200 eV in the figures. The present DCS can be compared with the experimental results of Sohn *et al.*,[27] at impact energies below 5 eV, with Michelin *et al.*[35] at energies above 30 eV, and Hoffman *et al.*[29] below 10 eV at an scattering angle of 135°. We also provide comparison with a range of other theoretical calculations, those of Raj and Tomar,[30] Lynch *et al.*,[31] Bettega *et al.*,[32,33] Gianturco and Stoecklin,[34] and Michelin *et al.*[35]

Between 1.2 and 10 eV the angular dependence of the cross section undergoes some significant changes, progressing from a strong forward scattering (1.2 eV) distribution through an essentially isotropic region, around 3 eV, before becoming dominated again by forward scattering at 10 eV. In the process, the minima in the cross section, which occurs at ∼100° at 1.2 eV, develops into several shallow minima at around 30° and 120°, before again reverting to a dominant single minimum at ∼120° and 10 eV. The behavior at lower energies is no doubt driven by several low energy resonances which have been revealed in previous experimental and theoretical studies. These include a $^2\Pi$ resonance at 1.2–1.33 eV and overlapping $^2\Sigma$ and $^2\Delta$ resonances at around 3.7 eV.[29] In general, the angular distribution of the scattered electron reflects the specific angular momentum involved with a shape resonance. In the case of scattering around 1–3 eV the $^2\Pi$ shape resonance contributes to the elastic DCS, via trapping of the incident electron into a π^* orbital through the $\ell = 1$ angular momentum centrifugal barrier. This is not reflected directly in the measured elastic DCS, though the observed behavior may be due to an additional, significant contribution from *d*-wave ($\ell = 2$) scattering, moderated by contributions from the other partial waves.

Between 15 and 60 eV the cross section returns to be dominated by forward scattering but there is also the development of a dual minima in the cross section at ∼60 and 120°—indicative of d-wave scattering. Between 60 and 200 eV the double minima vanish leaving again a strong forward peaking to the cross section and a single minimum at around 110°–120°.

In Figures 2(a)–2(d) we compare, in more detail, between the present experiment and other experiments and theories at four selected energies, 2.0, 5.0, 20, and 100 eV. At 2 eV (Figure 2(a)), the agreement between the present data and that of Sohn *et al.*[27] is excellent across the common range of angles. The best agreement with theory is shown with the calculation of Gianturco and Stoecklin,[34] particularly for scattering angles lower than about 80°. None of the other calculations reproduce all of the essential features of the experimental DCS. At 5.0 eV (Figure 2(b)) the general level of agreement between experiment and theory is considerably better, with all calculations reproducing the overall behavior of the DCS, with the IAM-SCAR calculation being perhaps the best of all across the angular range. Considering now 20 eV, Figure 2(c), all of the theoretical calculations are once again in good overall agreement with the experiment, although the CMS method does not predict the occurrence of the first minimum at around 70°. Finally, at 100 eV, Figure 2(d), there is excellent agreement between the present measurements and those of Michelin *et al.*,[35] and very good accord between our experiment and the IAM-SCAR result, the SMC calculation of Michelin *et al.*[35] and the CMS calculation of Raj and Tomar.[30]

In Figure 3(a), the integral elastic cross section (Q_e) derived from the present DCS are compared with other total elastic measurements and calculations. The agreement between the various experiments is excellent—roughly at the ±15% level across the whole energy range. Best agreement between the present measurements and theory is seen with the

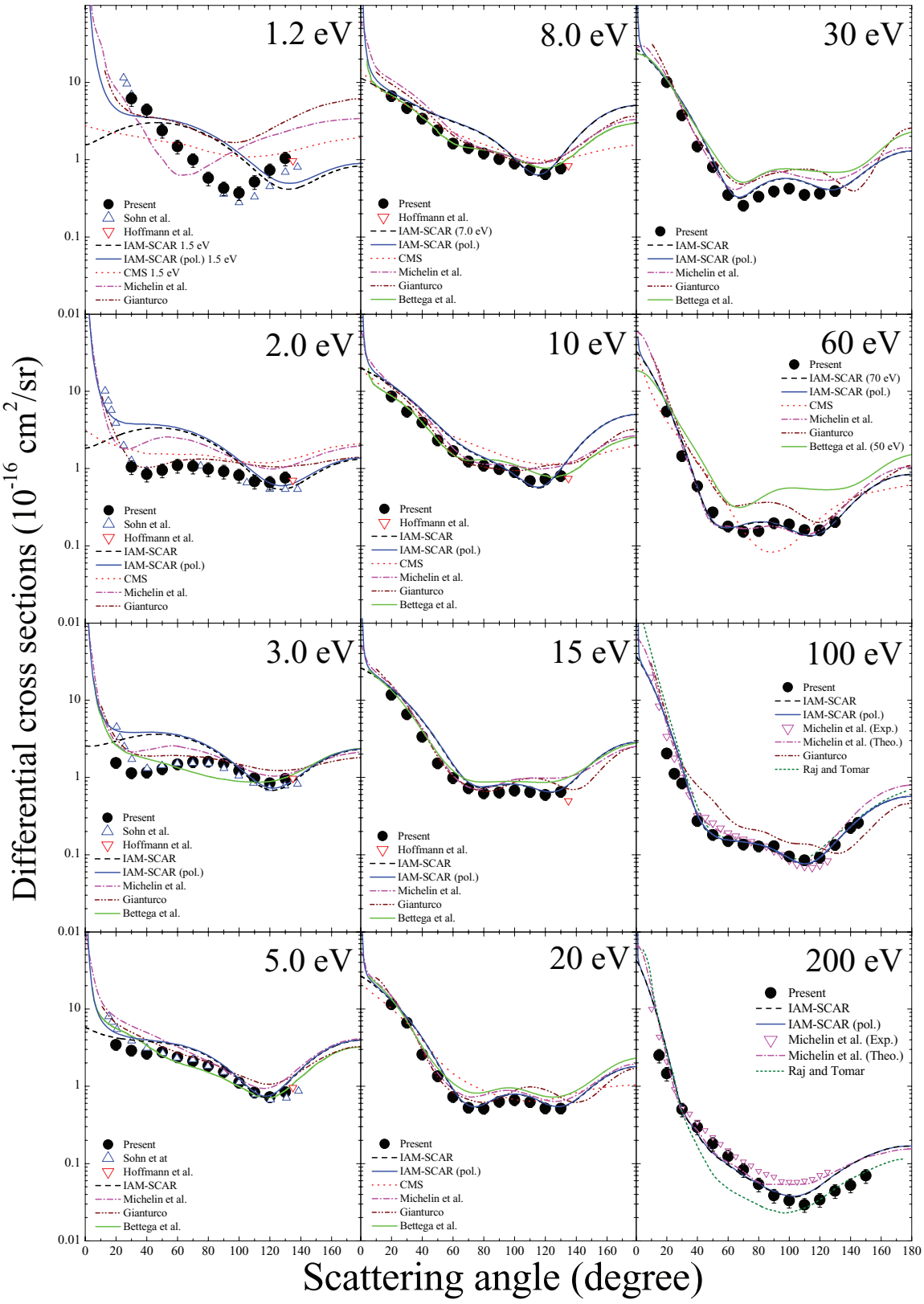

FIG. 1. Elastic differential cross sections (10^{-16} cm^2 sr^{-1}) for OCS (10^{-16} cm^2 sr^{-1}) at energies between 1.2 and 200 eV. The present measurements are compared to previous experiment and theory (see individual panels for details).

calculations of Lynch *et al.*[31] and Bettega *et al.*,[33] although it could be said that all of the theoretical calculations provide a reasonable description of the energy dependence and magnitude of the integral elastic cross section, including the present IAM-SCAR and CMS calculations.

In Figure 3(b) we make comparisons between the present data and calculations and previous (measured and calculated) grand total cross sections. The "present data" in this case takes two forms. At low energies (<4 eV) it represents a sum of our integral elastic cross sections with the vibrational cross sections from Sohn *et al.*[27] At higher energies, the present grand total cross section is the sum of our experimental integral elastic cross section together with the total inelastic cross section calculated within the IAM-SCAR formalism. Within a reasonable margin of error (∼10%), the present result provides a good description of the grand total cross section in both the energy dependence, and magnitude, below 30 eV. It exhibits an increasing trend in magnitude due to the $^2\Pi$ resonance at ∼1.3 eV and a weak maximum due to the overlapping $^2\Sigma$ and $^2\Delta$ resonances at 3.7 eV. These summed total cross sections are also in fairly good agreement with the previous experimental data. Once again the general utility of the IAM-SCAR theory in accurately predicting the overall cross section is demonstrated in Figure 3(b). For completeness we also show in Figure 3(b) the contributions to the inelastic and ionization cross sections from other various calculations and experiments.

B. CS_2

Figure 4 shows the overall behavior of the elastic differential cross sections for CS_2 at energies between 1.5 and 200 eV. The present calculated results (IAM-SCAR and CMS) are also presented and compared, as are the Schwinger variational calculations of Lee *et al.*,[41] the SMC results of Bettega *et al.*,[42,43] the results from the calculation of Gianturco and Stoecklin[44] and the IAM calculations of Raj and Tomar.[30] We also compare with the other available experimental results, those of Sohn *et al.*[27] and Allan.[39] We note that the measurements of Allan[39] were obtained at a fixed angle (135°) and mainly focused on the high-resolution study of near threshold features in the vibrational excitation. The present experimental DCS, and the integral elastic cross sections derived from them, are provided in Table II.

The overall behavior of the DCS as a function of energy in Figure 4 shows some similarities, particularly at low energies, to that exhibited from OCS. At the lowest energy

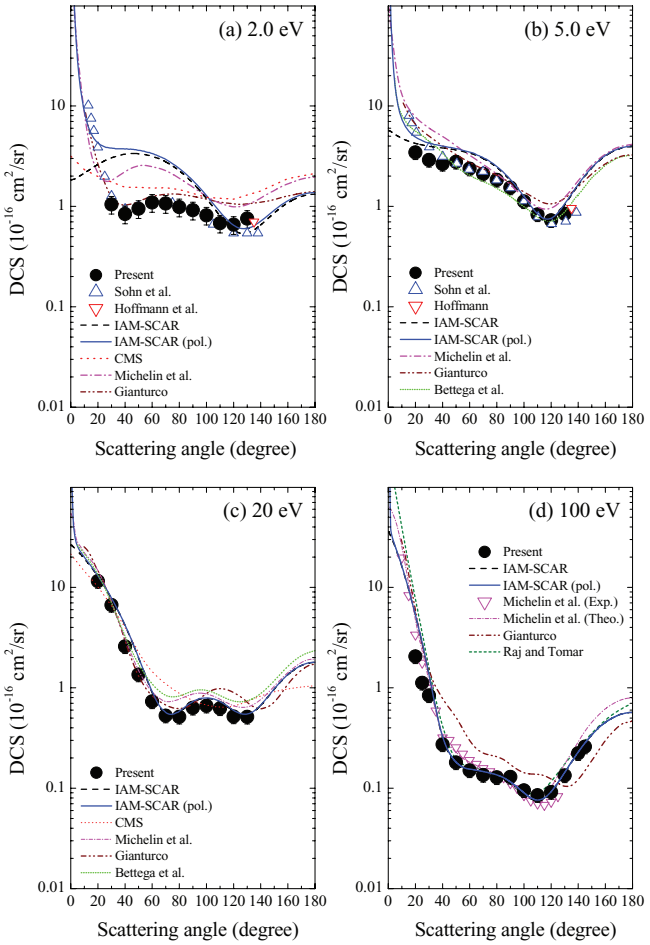

FIG. 2. Elastic differential cross sections (10^{-16} cm^2 sr^{-1}) for OCS at energies of (a) 2 eV, (b) 5 eV, (c) 20 eV, and (d) 100 eV. The present measurements are compared to previous experiment and theory (see individual panels for details).

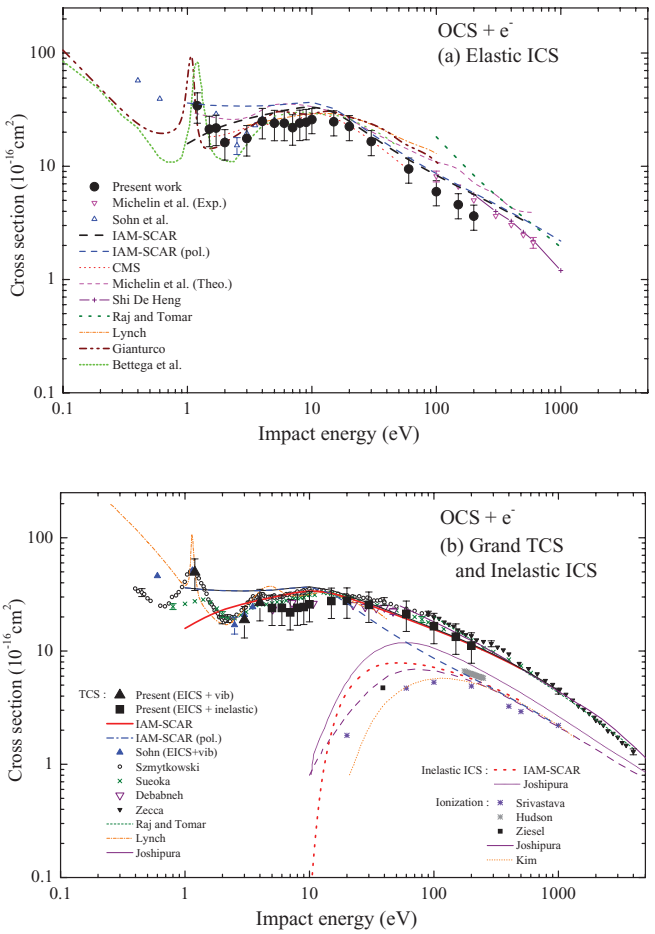

FIG. 3. (a) Elastic Integral cross sections (10^{-16} cm^2) for OCS (see legend for details). The present data are compared to previous experiment and theory. (b) Total cross sections (10^{-16} cm^2) for OCS (see legend for details). The present derived data are compared to previous experiment and theory.

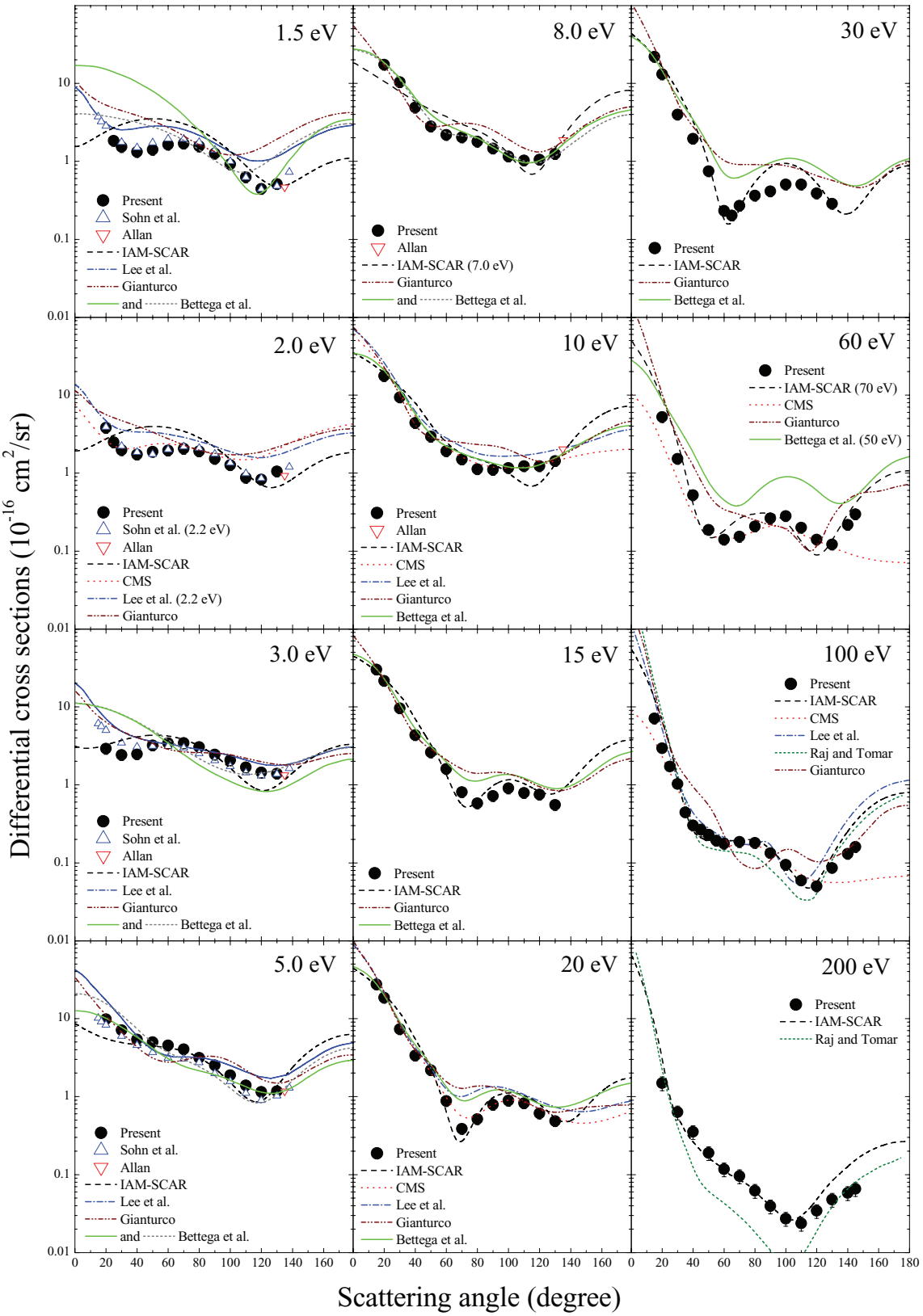

FIG. 4. Elastic differential cross sections (10^{-16} cm^2 sr^{-1}) for CS_2 at energies between 1.5 and 200 eV. The present measurements are compared to previous experiment and theory (see individual panels for details).

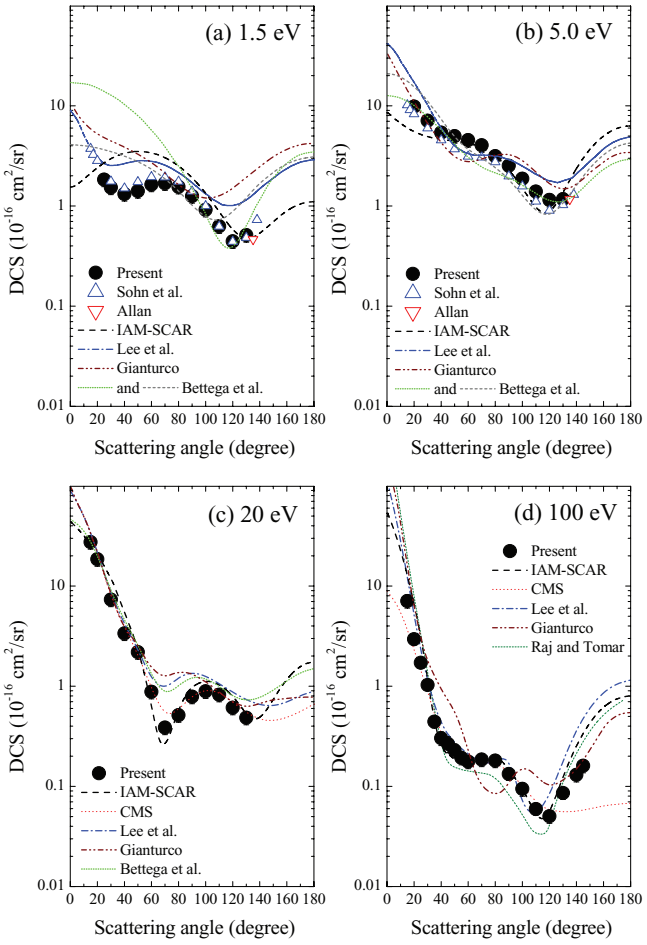

FIG. 5. Differential elastic scattering cross sections (10^{-16} cm^2 sr^{-1}) for CS_2 at (a) 1.5 eV, (b) 5 eV, (c) 20 eV, and (d) 100 eV. The present measurements are compared to previous experiment and theory (see individual panels for details).

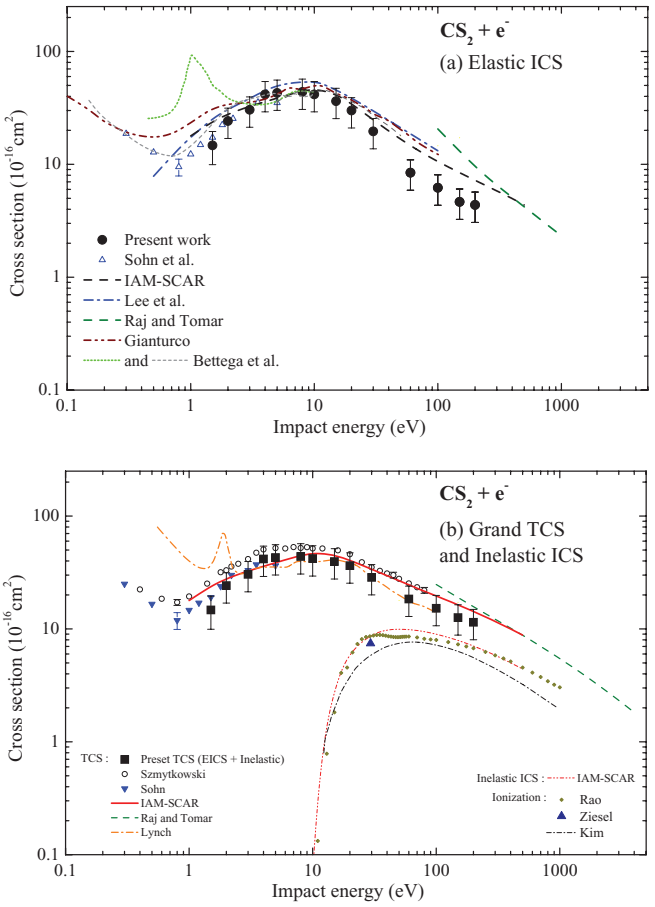

FIG. 6. (a) Elastic Integral cross sections (10^{-16} cm^2) for CS_2 (see legend for details). The present data are compared to previous experiment and theory. (b) Total scattering cross section for CS_2 (see legend for detail). The present derived data are compared to previous experiment and theory.

(1.5 eV) the DCS exhibits relatively strong forward scattering, particularly if one considers the extended angular range data of Sohn *et al.*[27] This quickly flattens out by ∼3 eV where a similar pair of week minima is observed at around 30° and 120°, as for OCS. Beyond 5 eV the DCS once again becomes quite strongly forward peaked with a single, large-angle minima, and at intermediate energies, above ∼15 eV, two minima are clearly discernible, suggesting therefore some dominance of d-wave scattering. By 200 eV the cross section has a single minimum at 110° and its size extends (for the angles measured) over roughly two orders of magnitude. The agreement with the experimental values of Sohn *et al.*[27] is excellent at all common energies, while the various theories, in general, provide a very good description of the DCS, particularly as the energy increases above ∼20 eV.

In Figure 5 we now provide a more detailed comparison with a selection of DCS results at energies of 1.5, 5, 20, and 100 eV (Figures 5(a)–5(d), respectively). At 1.5 eV we see, as noted above, excellent agreement between the present experimental cross section and that of Sohn *et al.*[27] The SVIM calculation of Lee *et al.*[41] provides a good overall description of the shape of the DCS but it is generally higher in magnitude, with the exception of the most forward angles we see good agreement between this calculation and the data of Sohn *et al.*[27] Perhaps not surprisingly, the IAM-SCAR calculation does not predict the DCS well at this energy, with a completely different angular dependence and magnitude at low angles. However, above about 100°, this theory is in relatively good accord with experiment. At 5 eV (Figure 5(b)) the agreement with Sohn *et al.*[27] is again very good, although some small differences in magnitude occur for scattering at mid angles (∼60°). As at lower energies, the IAM-SCAR, SMC[42,43] and SVIM[41] theories provide good agreement with experiment in different angular ranges, with the SVIM calculation in better agreement at angles below 60°, while the IAM-SCAR result agrees better at larger angles.

At 20 eV (Figure 5(c)) all five calculations agree with experiment very well for angles less than 60°. Above this, the IAM-SCAR method provides the best description of the experimental data, passing through the experimental points at essentially all angles. Finally, at an energy of 100 eV (Figure 5(d)), the minimum at around 60° has almost disappeared while that at 120° is now quite deep, with the overall measured cross section occupying more than two orders of magnitude in scale. At this energy we can compare with four calculated cross sections and again, all provide an excellent agreement at smaller scattering angles, with the best overall agreement being found with the IAM-SCAR approach, although the SVIM cross section of Lee *et al.*[41] and the IAM

TABLE I. Differential (10^{-16} cm^2/sr) and integral cross sections (10^{-16} cm^2) for elastic scattering from the OCS molecule. Errors on the DCS are typically 15%–20%, while on the ICS they are usually in the range 25%–30%. The actual absolute errors in each case are given in parentheses.

Angle	Energy (eV)																		
(deg)	1.2	1.5	1.7	2	3	4	5	6	7	8	9	10	15	20	30	60	100	150	200
20	…	…	…	…	1.541 (±0.23)	3.032 (±0.45)	3.439 (±0.52)	4.231 (±0.63)	4.728 (±0.71)	6.657 (±1.00)	7.588 (±1.14)	8.615 (±1.29)	11.712 (±1.76)	11.528 (±1.73)	10.122 (±1.52)	5.486 (±0.83)	2.048 (±0.31)	1.987 (±0.30)	1.460 (±0.22)
30	6.134 (±0.92)	2.312 (±0.35)	2.711 (±0.41)	1.003 (±0.15)	1.138 (±0.17)	2.349 (±0.35)	2.893 (±0.43)	3.400 (±0.51)	3.641 (±0.55)	4.673 (±0.70)	5.095 (±0.76)	5.460 (±0.82)	6.554 (±0.98)	6.661 (±1.00)	3.764 (±0.57)	1.449 (±0.22)	0.838 (±0.13)	0.556 (±0.09)	0.502 (±0.08)
40	4.385 (±0.66)	1.674 (±0.25)	1.679 (±0.25)	0.817 (±0.13)	1.152 (±0.17)	2.474 (±0.37)	2.640 (±0.40)	3.088 (±0.46)	3.077 (±0.46)	3.392 (±0.51)	3.443 (±0.52)	3.941 (±0.59)	3.349 (±0.50)	2.583 (±0.39)	1.484 (±0.22)	0.592 (±0.09)	0.272 (±0.04)	0.335 (±0.05)	0.295 (±0.05)
50	2.375 (±0.36)	1.345 (±0.20)	1.373 (±0.21)	0.948 (±0.14)	1.282 (±0.19)	2.283 (±0.34)	2.776 (±0.42)	2.526 (±0.38)	2.198 (±0.33)	2.405 (±0.36)	2.258 (±0.34)	2.314 (±0.35)	1.520 (±0.23)	1.353 (±0.20)	0.802 (±0.12)	0.270 (±0.04)	0.180 (±0.03)	0.238 (±0.04)	0.180 (±0.03)
60	1.480 (±0.23)	1.199 (±0.18)	1.359 (±0.20)	1.092 (±0.17)	1.479 (±0.22)	2.527 (±0.38)	2.370 (±0.36)	2.186 (±0.33)	1.869 (±0.28)	1.613 (±0.24)	1.510 (±0.23)	1.685 (±0.25)	0.980 (±0.15)	0.731 (±0.11)	0.351 (±0.05)	0.178 (±0.03)	0.150 (±0.03)	0.177 (±0.03)	0.123 (±0.02)
70	0.994 (±0.15)	0.911 (±0.14)	1.278 (±0.19)	1.066 (±0.16)	1.574 (±0.24)	2.428 (±0.36)	2.109 (±0.32)	1.814 (±0.27)	1.464 (±0.22)	1.421 (±0.21)	1.208 (±0.18)	1.236 (±0.19)	0.723 (±0.11)	0.527 (±0.08)	0.254 (±0.04)	0.152 (±0.03)	0.135 (±0.02)	0.127 (±0.02)	0.083 (±0.01)
80	0.575 (±0.09)	0.745 (±0.12)	1.090 (±0.17)	0.984 (±0.15)	1.599 (±0.24)	2.116 (±0.32)	1.835 (±0.28)	1.649 (±0.25)	1.348 (±0.20)	1.202 (±0.18)	1.092 (±0.16)	1.089 (±0.16)	0.622 (±0.09)	0.513 (±0.08)	0.332 (±0.05)	0.156 (±0.03)	0.128 (±0.02)	0.096 (±0.02)	0.054 (±0.01)
90	0.428 (±0.07)	0.625 (±0.10)	0.997 (±0.15)	0.916 (±0.14)	1.500 (±0.23)	1.738 (±0.26)	1.536 (±0.23)	1.277 (±0.19)	1.177 (±0.18)	1.021 (±0.15)	1.022 (±0.15)	0.984 (±0.15)	0.638 (±0.10)	0.631 (±0.10)	0.388 (±0.06)	0.196 (±0.03)	0.129 (±0.02)	0.081 (±0.01)	0.039 (±0.01)
100	0.371 (±0.06)	0.564 (±0.09)	0.918 (±0.14)	0.815 (±0.12)	1.220 (±0.18)	1.440 (±0.22)	1.117 (±0.17)	1.058 (±0.16)	0.895 (±0.13)	0.893 (±0.13)	0.890 (±0.13)	0.898 (±0.13)	0.675 (±0.10)	0.661 (±0.10)	0.423 (±0.05)	0.190 (±0.03)	0.095 (±0.02)	0.062 (±0.01)	0.033 (±0.01)
110	0.516 (±0.08)	0.532 (±0.08)	0.956 (±0.15)	0.679 (±0.10)	0.976 (±0.15)	1.034 (±0.16)	0.829 (±0.12)	0.706 (±0.11)	0.633 (±0.09)	0.737 (±0.11)	0.695 (±0.10)	0.691 (±0.10)	0.647 (±0.10)	0.623 (±0.09)	0.351 (±0.06)	0.161 (±0.03)	0.085 (±0.02)	0.055 (±0.01)	0.029 (±0.01)
120	0.729 (±0.11)	0.659 (±0.10)	1.118 (±0.17)	0.658 (±0.10)	0.839 (±0.13)	0.845 (±0.13)	0.725 (±0.11)	0.677 (±0.10)	0.560 (±0.08)	0.649 (±0.10)	0.634 (±0.10)	0.730 (±0.11)	0.594 (±0.09)	0.517 (±0.08)	0.364 (±0.06)	0.159 (±0.03)	0.091 (±0.02)	0.065 (±0.02)	0.034 (±0.01)
130	1.038 (±0.16)	0.829 (±0.13)	1.381 (±0.21)	0.755 (±0.12)	0.960 (±0.15)	1.003 (±0.15)	0.843 (±0.13)	0.801 (±0.12)	0.676 (±0.10)	0.769 (±0.12)	0.774 (±0.12)	0.801 (±0.12)	0.650 (±0.10)	0.514 (±0.08)	0.393 (±0.06)	0.203 (±0.03)	0.134 (±0.02)	0.085 (±0.02)	0.044 (±0.01)
140	…	…	…	…	…	…	…	…	…	…	…	…	…	…	…	…	0.222 (±0.03)	0.126 (±0.02)	0.052 (±0.01)
145	…	…	…	…	…	…	…	…	…	…	…	…	…	…	…	…	0.259 (±0.04)	0.133 (±0.02)	…
150	…	…	…	…	…	…	…	…	…	…	…	…	…	…	…	…	…	…	0.070 (±0.01)
ICS	34.251 (±10.3)	21.261 (±6.4)	21.741 (±6.5)	16.203 (±4.9)	17.600 (±5.3)	24.950 (±7.5)	23.988 (±7.4)	24.005 (±7.2)	21.913 (±6.6)	24.064 (±7.2)	24.453 (±7.3)	25.844 (±7.7)	24.722 (±6.2)	22.427 (±5.6)	16.532 (±4.1)	9.453 (±2.4)	5.965 (±1.5)	4.579 (±1.1)	3.630 (±0.9)

TABLE II. Differential (10^{-16} cm^2/sr) and integral cross sections (10^{-16} cm^2) for elastic scattering from the CS_2 molecule. Errors on the DCS are typically 15%–20%, while on the ICS they are usually in the range 25%–30%. The actual absolute errors in each case are given in parentheses.

Angle	Energy (eV)													
(deg)	1.5	2	3	4	5	8	10	15	20	30	60	100	150	200
15	…	…	…	…	…	…	…	30.107 (±4.52)	27.424 (±4.11)	21.926 (±3.30)	…	7.089 (±1.10)	…	…
20	…	3.797 (±0.57)	2.899 (±0.43)	7.389 (±1.11)	9.833 (±1.47)	17.334 (±2.60)	17.504 (±2.63)	21.503 (±3.23)	18.531 (±2.78)	13.037 (±1.96)	5.234 (±0.80)	2.943 (±0.44)	1.369 (±0.21)	1.488 (±0.22)
25	1.834 (±0.28)	2.482 (±0.37)	…	…	…	…	…	…	…	…	…	…	…	…
30	1.528 (±0.23)	1.969 (±0.30)	2.420 (±0.36)	5.496 (±0.82)	7.102 (±1.07)	10.343 (±1.55)	9.336 (±1.40)	9.557 (±1.43)	7.324 (±1.10)	3.962 (±0.60)	1.522 (±0.23)	1.027 (±0.15)	0.454 (±0.07)	0.629 (±0.10)
40	1.317 (±0.20)	1.728 (±0.26)	2.479 (±0.37)	4.341 (±0.65)	5.398 (±0.81)	4.908 (±0.74)	4.382 (±0.66)	4.342 (±0.65)	3.364 (±0.50)	1.950 (±0.30)	0.520 (±0.08)	0.303 (±0.05)	0.325 (±0.05)	0.353 (±0.05)
50	1.409 (±0.21)	1.876 (±0.28)	3.202 (±0.48)	4.218 (±0.63)	4.972 (±0.75)	2.808 (±0.42)	2.935 (±0.44)	2.610 (±0.39)	2.184 (±0.33)	0.748 (±0.11)	0.187 (±0.03)	0.229 (±0.03)	0.199 (±0.03)	0.189 (±0.03)
60	1.636 (±0.25)	1.947 (±0.29)	3.415 (±0.51)	4.822 (±0.72)	4.536 (±0.68)	2.185 (±0.33)	1.909 (±0.29)	1.594 (±0.24)	0.878 (±0.13)	0.233 (±0.03)	0.140 (±0.03)	0.177 (±0.03)	0.144 (±0.02)	0.117 (±0.02)
70	1.684 (±0.23)	2.049 (±0.31)	3.447 (±0.52)	4.370 (±0.66)	4.036 (±0.61)	2.036 (±0.31)	1.496 (±0.22)	0.806 (±0.12)	0.387 (±0.06)	0.270 (±0.04)	0.153 (±0.03)	0.185 (±0.03)	0.121 (±0.02)	0.096 (±0.01)
80	1.555 (±0.19)	1.906 (±0.29)	3.053 (±0.46)	3.809 (±0.57)	3.137 (±0.47)	1.794 (±0.27)	1.120 (±0.17)	0.580 (±0.09)	0.514 (±0.08)	0.364 (±0.05)	0.207 (±0.02)	0.181 (±0.03)	0.081 (±0.01)	0.062 (±0.01)
90	1.255 (±0.14)	1.525 (±0.23)	2.444 (±0.37)	3.042 (±0.46)	2.520 (±0.38)	1.457 (±0.22)	1.100 (±0.16)	0.720 (±0.11)	0.787 (±0.12)	0.412 (±0.06)	0.263 (±0.02)	0.133 (±0.02)	0.051 (±0.01)	0.039 (±0.01)
100	0.917 (±0.18)	1.262 (±0.19)	2.070 (±0.31)	2.341 (±0.35)	1.874 (±0.28)	1.159 (±0.17)	1.163 (±0.17)	0.902 (±0.14)	0.889 (±0.13)	0.505 (±0.08)	0.281 (±0.03)	0.094 (±0.01)	0.027 (±0.01)	0.027 (±0.01)
110	0.626 (±0.09)	0.873 (±0.13)	1.676 (±0.25)	1.837 (±0.28)	1.394 (±0.21)	1.024 (±0.15)	1.227 (±0.18)	0.789 (±0.12)	0.820 (±0.12)	0.506 (±0.08)	0.200 (±0.04)	0.059 (±0.01)	0.020 (±0.01)	0.024 (±0.01)
120	0.444 (±0.07)	0.824 (±0.12)	1.440 (±0.22)	1.591 (±0.24)	1.151 (±0.17)	1.053 (±0.16)	1.230 (±0.18)	0.751 (±0.11)	0.611 (±0.10)	0.389 (±0.06)	0.140 (±0.04)	0.050 (±0.01)	0.028 (±0.01)	0.034 (±0.01)
130	0.511 (±0.08)	1.048 (±0.16)	1.391 (±0.21)	1.411 (±0.21)	1.170 (±0.18)	1.242 (±0.19)	1.425 (±0.21)	0.554 (±0.08)	0.484 (±0.07)	0.287 (±0.04)	0.122 (±0.02)	0.086 (±0.01)	0.043 (±0.01)	0.048 (±0.01)
140	…	…	…	…	…	…	…	…	…	…	0.217 (±0.03)	0.130 (±0.02)	0.078 (±0.01)	0.058 (±0.01)
145	…	…	…	…	…	…	…	…	…	…	0.297 (±0.04)	0.161 (±0.02)	…	0.066 (±0.01)
150	…	…	…	…	…	…	…	…	…	…	…	…	0.093 (±0.01)	…
ICS (Error)	14.733 (±4.4)	24.205 (±7.3)	30.443 (±9.1)	41.666 (±12.5)	42.912 (±12.8)	43.802 (±13.1)	41.662 (±10.4)	36.284 (±9.1)	29.989 (±7.5)	19.603 (±4.9)	8.431 (±2.1)	6.203 (±1.6)	4.651 (±1.2)	4.371 (±1.1)

calculation of Raj and Tomar[30] also provide a quite good comparison with experiment. At larger angles the CMS cross section is quite different to the experiment.

In Fig. 6(a), the integral elastic cross sections which have been derived from the present DCS are compared with results from other measurements and calculations. Our Q_e agrees well with the previous result of Sohn *et al.*[27] below 5 eV, but no other experimental data are available for comparison from 8 to 200 eV. Six theoretical approaches are available for comparison, those of Lynch *et al.*,[31] Lee *et al.*,[41] Bettega *et al.*,[42,43] Gianturco and Stoecklin,[44] and Raj and Tomar,[30] as well as the present IAM-SCAR calculation. The calculation of Raj and Tomar[30] (only above 100 eV) considerably overestimates the experimental measurement. The other five calculations are in good agreement with the experiment in the region between 5 and 30 eV, but all are slightly larger in magnitude than experiment at energies, both high and low, either side of this region. The calculation of Lynch *et al.*[31] shows a strong shape resonance at around 2 eV (see Figure 6(b)), which is neither indicated in the present experimental integral cross section nor in that of Sohn *et al.*[27]

Figure 6(b) shows the present grand total scattering cross section, obtained by adding together the experimental elastic integral cross section, and the total inelastic cross section, calculated in the IAM-SCAR approach. This cross section is compared with other experimental and theoretical values and we also show the present total inelastic cross section from the IAM-SCAR method compared with the available ionization and excitation measurements. The present total cross section is in good agreement with the measured values of Szmytkowski,[37] particularly at mid to higher energies, where although slightly lower in magnitude, the two results overlap within their estimated errors. At lower energies we may expect the present result to be lower than that

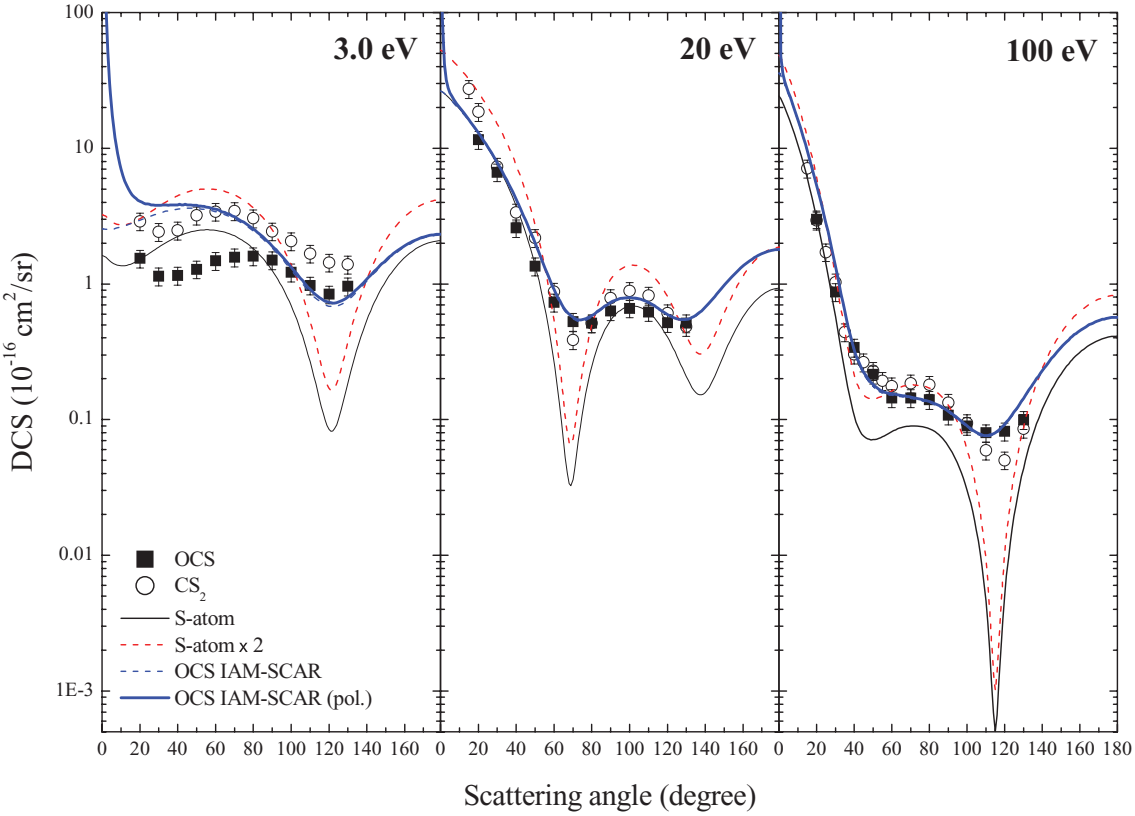

FIG. 7. Comparison of the elastic DCS of OCS and CS_2 with the IAM-SCAR result of that for the S atom and twice the DCS of the S atom. See also the legend in the figure.

of Szmytkowski's, as our result does not include vibrational excitation. The agreement with the IAM-SCAR cross section is very good across the whole energy range.

C. Comparison of the DCSs for OCS, CS_2, and atomic-S

As three representative cases, the angular behavior of the DCS for OCS and CS_2 are illustrated at 3, 20, and 100 eV in Figure 7, and compared with the calculated DCS for atomic sulphur and that for twice the DCS of atomic sulphur. As an initial observation it would appear that, at these energies, the shape of the angular distribution is largely derived from the atomic S or S_2 scattering. At the higher energies, 20 eV and 100 eV, the DCS for OCS and CS_2 largely overlap each other and show a similar angular distribution as for atomic S, with the "filling-in" of the minimum in the molecular cases being most likely due to their molecular structure. This seems a reasonable assumption, and the reason why the molecular DCS are relatively smoother is most likely due to their random molecular orientations in the gas. Of course, the angular scattering that is observed for the forward scattering angles is due to the long range interactions, such as the dipole polarizability and the permanent dipole moment. Although the variation of the molecular polarizability is from 38.5 a.u. (OCS) to 59.8 a.u. (CS_2), those effects are not clearly visible within the present measurements. Further investigations may be beneficial for the forward scattering at lower impact energies. As is evident from the level of agreement between the present experimental results and the IAM-SCAR calculation, the atomic-like effects are dominant in the scattering dynamics, even for the molecular structures. These features have been observed in several cases[45–48] at higher impact energies above 50 eV. But, it is worth noting that the atomic form factor of the S atom (atomic number: 16) plays an important role in the elastic scattering from OCS and CS_2, more so than the other constituents of C (6) and O (8), over the impact energy from a few eV to 200 eV.

V. SUMMARY

We have provided absolute elastic DCS for OCS and CS_2 in the energy range of 1.2–200 eV and over the scattering angles 20° to 150°. Corresponding theoretical cross sections, calculated within the IAM-SCAR, and the CMS approaches, are found to be in good agreement with the experimental data above 10 eV, as are the results of a number of other calculations, some of which are *ab initio*. Good agreement is also found between experiment and theory at the integral elastic and grand total cross section levels. Atomic-like behavior in these scattering systems is shown here, and is highlighted by comparing the OCS and CS_2 elastic cross sections to recent theoretical results on atomic sulphur at intermediate and higher impact energies.

ACKNOWLEDGMENTS

The present work has been supported by the Japanese Ministry of Education, Sport, Culture and Technology and

the Australian Research Council through its Centers of Excellence program. PL-V acknowledges his Visiting Professor position at Sophia University, Tokyo, Japan and also the Portuguese PEst-OE/FIS/UI0068/2011 grant. This work forms part of the EU/ESF COST Action CM0805 programme "The Chemical Cosmos." M.J.B. and S.J.B. acknowledge the JSPS for provision of a Senior Fellowship, and the University of Malaya for their hospitality as Visiting Professor F. Blanco and Professor G. García acknowledge partial financial support of the Spanish Ministerio de Economia y Competitividad through Project No. FIS2009-10245 as well as the EU/ESF COST Action MP1002.

[1]S. K. Srivastava, H. Tanaka, and A. Chutjian, J. Chem. Phys. **69**, 1493 (1978).
[2]H. Tanaka, L. Boesten, D. Matsunaga, and T. Kudo, J. Phys. B **21**, 1255 (1988).
[3]M. Kitajima, Y. Sakamoto, S. Watanabe, T. Suzuki, T. Ishikawa, H. Tanaka, and M. Kimura, Chem. Phys. Lett. **309**, 414 (1999).
[4]P. Limão-Vieira, S. Eden, P. A. Kendall, N. J. Mason, and S. V. Hoffmann, Chem. Phys. Lett. **366**, 343 (2002).
[5]E. A. Drage, P. Cahillane, S. V. Hoffmann, N. J. Mason, and P. Limão-Vieira, Chem. Phys. **331**, 447 (2007).
[6]M. Pham, J.-F. Mueller, G. P. Brasseur, C. Granier, and G. Megie, J. Geophys. Res. **100**, 26061, doi:10.1029/95JD02095 (1995).
[7]E. Kjellstrom, J. Atoms. Chem. **29**, 151 (1998).
[8]M. Chin and D. D. Davis, J. Geophys. Res. **100**, 8993, doi:10.1029/95JD00275 (1995).
[9]J. E. Johnson and T. S. Bates, J. Geophys. Res. **98**, 23443, doi:10.1029/92JD01911 (1993).
[10]D. C. Thornton, A. R. Bandy, B. W. Blomquist, and B. E. Anderson, J. Geophys. Res. **101**, 1873, doi:10.1029/95JD00617 (1996).
[11]B. Bezard, C. De Bergh, D. Crisp, and J. P. Maillard, Nature (London) **345**, 508 (1990).
[12]E. Lellouch, G. Paubert, R. Moreno, M. Festou, B. Bezard, D. Bockelee-Morven, P. Colon, J. Crovisier, T. Encrenac *et al.*, Nature (London) **373**, 592 (1995).
[13]M. E. Palumbo, A. G. G. M. Tielens, and A. T. Tokunaga, Astrophys. J. **449**, 674 (1995).
[14]M. E. Palumbo, T. R. Geballe, and A. G. G. M. Tielens, Astrophys. J. **479**, 839 (1997).
[15]Y. Ueno, M. S. Johnson, S. O. Danielache, C. Eskebjerg, A. Pandey, and N. Yoshida, Proc. Natl. Acad. Sci. U.S.A. **106**, 14784 (2009).
[16]Kanto Denka Kogyo Co., Ltd., private communication (2010).
[17]C. B. Cosmovici and S. Ortolani, Nature (London) **310**, 122 (1984).
[18]*CRC Handbook of Chemistry and Physics*, 88th ed., edited by D. R. Lide (CRC, Boca Raton, FL, 2007–2008).
[19]K. Tanaka, H. Ito, K. Harada, and T. Tanaka, J. Chem. Phys. **80**, 5893 (1984).
[20]W. J. Hehere, L. Radom, P. V. R. Scheyer, and J. A. Pople, *Ab initio Molecular Orbital Theory* (Wiley, New York, 1986), p. 174.
[21]C. Szmytkowski, G. Karwasz, and K. Maciag, Chem. Phys. Lett. **107**, 481 (1984).
[22]C. Szmytkowski, K. Maciag, G. Karwasz, and D. Filipovic, J. Phys. B **22**, 525 (1989).
[23]M. S. Dababneh, Y. F. Hsieh, W. E. Kauppila, C. K. Kwan, and T. S. Stein, in *Proceedings of III International Workshop on Positron (Electron) – Gas Scattering, Detroit*, edited by W. E. Kauppila *et al.* (World Scientific, 1986), p. 251.
[24]A. Zecca, J. C. Noguerira, G. P. Karwasz, and R. S. Brusa, J. Phys. B **28**, 477 (1995).
[25]O. Sueoka, K. Kimura, H. Tanaka, and M. Kitajima, J. Chem. Phys. **111**, 245 (1999).
[26]N. C. Jones, D. Field, S. L. Lunt, and J.-P. Ziesel, Phys. Rev. A **78**, 042714 (2008).
[27]W. Sohn, K.-H. Kochem, K. M. Scheuerlein, K. Jung, and H. Erhardt, J. Phys. B **20**, 3217 (1987).
[28]XXI International Conference on Physics of Electronic and Atomic Collisions, Abstracts of Contributed Papers I, edited by Y. Itikawa *et al.* (1999), p. 286.
[29]T. H. Hoffmann, H. Hotop, and M. Allan, J. Phys. B **41**, 195202 (2008).
[30]D. Raj and S. Tomar, J. Phys. B **30**, 1989 (1997).
[31]M. G. Lynch, D. Dill, J. Siegel, and J. L. Dehmer, J. Chem. Phys. **71**, 4249 (1979).
[32]M. H. F. Bettega, M. A. P. Lima, and L. G. Ferreira, Phys. Rev. A **70**, 062711 (2004).
[33]M. H. F. Bettega, M. A. P. Lima, and L. G. Ferreira, Aust. J. Phys. **53**, 399 (2000).
[34]F. A. Gianturco and T. Stoecklin, Chem. Phys. **332**, 145 (2007).
[35]S. K. Michelin, T. Kroin, I. Iga, M. G. P. Homem, H. S. Miglio, and M. T. Lee, J. Phys. B **33**, 3293 (2000).
[36]S. D. Heng, S. J. Feng, Z. Z. Lue, M. Heng, L. Y. Fang, and Y. X. Dong, Chin. Phys. **16**, 1655 (2007).
[37]C. Semytkowski, J. Phys. B **20**, 6613 (1987).
[38]N. C. Jones, D. Field, J.-P. Ziesel, and T. A. Field, Phys. Rev. Lett. **89**, 093201 (2002).
[39]M. Allan, J. Phys. B **36**, 2489 (2003).
[40]C. Semytkowski, Fizika **21**, 325 (1989).
[41]M. T. Lee, S. E. Michelin, T. Kroin, and E. Veitenheimer, J. Phys. B **32**, 3043 (1999).
[42]M. H. F. Bettega, M. A. P. Lima, and L. G. Ferreira, J. Phys. B **38**, 2087 (2005).
[43]M. H. F. Bettega, A. P. P. Natalense, M. A. P. Lima, and L. G. Ferreira, Braz. J. Phys. **30**, 189 (2000).
[44]F. A. Gianturco and T. Stoecklin, Eur. Phys. J. D. **42**, 85 (2007).
[45]M. A. Dillon, L. Boesten, H. Tanaka, M. Kimura, and H. Sato, J. Phys. B **26**, 3147 (1993).
[46]H. Kato, T. Asahina, H. Masui, M. Hoshino, H. Tanaka, H. Cho, O. Ingólfsson, F. Blanco, G. García, S. J. Buckman, and M. J. Brunger, J. Chem. Phys. **132**, 074309 (2010).
[47]P. Limão-Vieira, M. Horie, H. Kato, M. Hoshino, F. Blanco, G. García, S. J. Buckman, and H. Tanaka, J. Chem. Phys. **135**, 234309 (2011).
[48]H. Kato, A. Suga, M. Hoshino, F. Blanco, G. García, P. Limão-Vieira, M. J. Brunger, and H. Tanaka, J. Chem. Phys. **136**, 134313 (2012).
[49]H. Tanaka, T. Ishikawa, T. Masai, T. Sagara, L. Boesten, M. Takekawa, Y. Itikawa, and M. Kimura, Phys. Rev. A **57**, 1798 (1998).
[50]T. Shimanouchi, "Tables of molecular vibrational frequencies," NBS Ref. Data Ser. 39, Vol. I (U.S. Government Printing Office, Washington, DC, 1972).
[51]J. N. H. Brunt, G. C. King, and F. H. Read, J. Phys. B **10**, 1289 (1977).
[52]S. F. Wong and L. Dube, Phys. Rev. A **17**, 570 (1978).
[53]S. K. Srivastava, A. Chutjian, and S. Trajmar, J. Chem. Phys. **63**, 2659 (1975).
[54]J. Nickel, P. W. Zetner, G. Shen, and S. Trajmar, J. Phys. E **22**, 730 (1989).
[55]L. Boesten and H. Tanaka, At. Data Nucl. Data Tables **52**, 25 (1992).
[56]M. A. Khakoo and S. Trajmar, Phys. Rev. A **34**, 138 (1986).
[57]D. T. Alle, R. J. Gulley, S. J. Buckman, and M. J. Brunger, J. Phys. B **25**, 1533 (1992).
[58]F. Blanco and G. Garcia, Phys. Lett. A **295**, 178 (2002).
[59]F. Blanco and G. Garcia, Phys. Rev. A **67**, 022701 (2003).
[60]F. Blanco and G. Garcia, Phys. Lett. A **317**, 458 (2003).
[61]F. Blanco and G. Garcia, Phys. Lett. A **330**, 230 (2004).
[62]A. G. Sanz, M. C. Fuss, F. Blanco, F. Sebastianelli, F. A. Gianturco, and G. Garcia, J. Chem. Phys. **137**, 124103 (2012).
[63]G. Staszewska, D. W. Schwenke, D. Thirumalai, and D. G. Truhlar, Phys. Rev. A **28**, 2740 (1983).
[64]R. Cowan, *The Theory of Atomic Structure and Spectra* (University of California, London, 1981).
[65]M. E. Riley and D. G. Truhlar, J. Chem. Phys. **63**, 2182 (1975).
[66]X. Z. Zhang, J. F. Sun, and Y. F. Liu, J. Phys. B **25**, 1893 (1992).
[67]J. B. Maljkovic, A. R. Milosavljevic, F. Blanco, D. Sevic, G. Garcia, and B. P. Marinkovic, Phys. Rev. A **79**, 052706 (2009).
[68]F. Blanco and G. Garcia, Phys. Lett. A **360**, 707 (2007).
[69]A. Jain, J. Phys. B **21**, 905 (1988).
[70]A. Munoz, J. C. Oller, F. Blanco, J. D. Gorfinkiel, P. Limao-Vieira, and G. Garcia, Phys. Rev. A **76**, 052707 (2007).
[71]D. Dill and J. L. Dehmer, J. Chem. Phys. **61**, 692 (1974).
[72]M. Kimura and H. Sato, Comment At. Mol. Phys. **26**, 333 (1991).
[73]F. W Averill and D. E. Ellis, J. Chem. Phys. **59**, 6412 (1973).
[74]S. Hara, J. Phys. Soc. Jpn. **22**, 710 (1967).